Research Article | Vol. 8, No. 7 | 1 Jul 2018 | OPTICAL MATERIALS EXPRESS 1723
Optical Materials EXPRESS

Sb_2Te_3 thin film for the passive Q-switching of a Tm:$GdVO_4$ laser

Pavel Loiko,[1,2] Jakub Bogusławski,[3,4] Josep Maria Serres,[1] Esrom Kifle,[1] Maciej Kowalczyk,[3] Xavier Mateos,[1,*] Jarosław Sotor,[3] Rafał Zybała,[5] Krzysztof Mars,[6] Andrzej Mikuła,[6] Kamil Kaszyca,[7] Magdalena Aguiló,[1] Francesc Díaz,[1] Uwe Griebner,[8] and Valentin Petrov[8]

[1]*Física i Cristal·lografia de Materials i Nanomaterials (FiCMA-FiCNA)-EMaS, Dept. Química Física i Inòrganica, Universitat Rovira i Virgili (URV), Campus Sescelades, E-43007 Tarragona, Spain*
[2]*ITMO University, 49 Kronverkskiy pr., 197101 St. Petersburg, Russia*
[3]*Laser & Fiber Electronics Group, Faculty of Electronics, Wrocław University of Science and Technology, Wybrzeże S. Wyspiańskiego 27, 50-370 Wrocław, Poland*
[4]*Institute of Physical Chemistry, Polish Academy of Sciences, Kasprzaka 44-52, 01-224 Warsaw, Poland*
[5]*University Research Centre, Functional Materials, Warsaw University of Technology, Wołoska 141, 02-507 Warsaw, Poland*
[6]*Faculty of Material Science and Ceramics, AGH University of Science and Technology, A. Mickiewicza 30, 30-059 Kraków, Poland*
[7]*Institute of Electronic Materials Technology, Wolczynska 133, 01-919 Warsaw, Poland*
[8]*Max Born Institute for Nonlinear Optics and Short Pulse Spectroscopy, Max-Born-Str. 2a, D-12489 Berlin, Germany*
[*]*xavier.mateos@urv.cat*

Abstract: We report on the first application of an antimony telluride (Sb_2Te_3) thin film as a saturable absorber (SA) in a microchip laser. The 3–15 nm-thick Sb_2Te_3 films were deposited on glass substrates by pulsed magnetron sputtering and they were studied by SEM, X-ray diffraction, Raman and optical spectroscopy. The saturable absorption of the Sb_2Te_3 film was confirmed at 1.56 μm for ns-long pulses revealing low saturation intensity of 0.17 MW/cm^2. The microchip laser was based on a Tm:$GdVO_4$ crystal diode-pumped at ~802 nm. In the continuous-wave regime, this laser generated 3.54 W at 1905–1921 nm with a slope efficiency of 37%. The Q-switched laser generated a maximum average output power of 0.70 W at 1913 nm. The highest pulse energy of 3.5 μJ and the shortest pulse duration of 223 ns were obtained at the 200 kHz repetition rate.

© 2018 Optical Society of America under the terms of the OSA Open Access Publishing Agreement

OCIS codes: (140.3380) Laser materials; (140.3540) Lasers, Q-switched; (140.3070) Infrared and far-infrared lasers.

References and links

1. R. R. Nair, P. Blake, A. N. Grigorenko, K. S. Novoselov, T. J. Booth, T. Stauber, N. M. Peres, and A. K. Geim, "Fine structure constant defines visual transparency of graphene," Science **320**(5881), 1308 (2008).
2. G. Xing, H. Guo, X. Zhang, T. C. Sum, and C. H. A. Huan, "The physics of ultrafast saturable absorption in graphene," Opt. Express **18**(5), 4564–4573 (2010).
3. Q. Bao, H. Zhang, Y. Wang, Z. Ni, Y. Yan, Z. X. Shen, K. P. Loh, and D. Y. Tang, "Atomic-layer graphene as a saturable absorber for ultrafast pulsed lasers," Adv. Funct. Mater. **19**(19), 3077–3083 (2009).
4. W. B. Cho, J. H. Yim, S. Y. Choi, S. Lee, A. Schmidt, G. Steinmeyer, U. Griebner, V. Petrov, D. I. Yeom, K. Kim, and F. Rotermund, "Boosting the non linear optical response of carbon nanotube saturable absorbers for broadband mode-locking of bulk lasers," Adv. Funct. Mater. **20**(12), 1937–1943 (2010).
5. J. Boguslawski, J. Sotor, G. Sobon, R. Kozinski, K. Librant, M. Aksienionek, L. Lipinska, and K. M. Abramski, "Graphene oxide paper as a saturable absorber for Er- and Tm-doped fiber lasers," Photon. Res. **3**(4), 119–124 (2015).
6. Z. Sun, A. Martinez, and F. Wang, "Optical modulators with 2D layered materials," Nat. Photonics **10**(4), 227–238 (2016).

#326632 https://doi.org/10.1364/OME.8.001723
Journal © 2018 Received 21 Mar 2018; revised 15 May 2018; accepted 16 May 2018; published 4 Jun 2018

Optical Materials EXPRESS

7. J. M. Serres, P. Loiko, X. Mateos, H. Yu, H. Zhang, Y. Chen, V. Petrov, U. Griebner, K. Yumashev, M. Aguiló, and F. Díaz, "MoS_2 saturable absorber for passive Q-switching of Yb and Tm microchip lasers," Opt. Mater. Express **6**(10), 3262–3273 (2016).
8. J. Sotor, G. Sobon, M. Kowalczyk, W. Macherzynski, P. Paletko, and K. M. Abramski, "Ultrafast thulium-doped fiber laser mode locked with black phosphorus," Opt. Lett. **40**(16), 3885–3888 (2015).
9. C. Zhao, H. Zhang, X. Qi, Y. Chen, Z. Wang, S. Wen, and D. Tang, "Ultra-short pulse generation by a topological insulator based saturable absorber," Appl. Phys. Lett. **101**(21), 211106 (2012).
10. X. Wang, J. Xu, Y. Sun, Z. Zhu, Z. You, and C. Tu, "Near infrared passively Q-switched solid state laser based on Sb_2Te_3 topological insulator saturable absorber," J. Lumin. **192**, 1–5 (2017).
11. F. Zhang, S. Han, Y. Liu, Z. Wang, and X. Xu, "Dependence of the saturable absorption of graphene upon excitation photon energy," Appl. Phys. Lett. **106**(9), 091102 (2015).
12. J. E. Moore, "The birth of topological insulators," Nature **464**(7286), 194–198 (2010).
13. H. Zhang, C. X. Liu, X. L. Qi, X. Dai, Z. Fang, and S. C. Zhang, "Topological insulators in Bi_2Se_3, Bi_2Te_3 and Sb_2Te_3 with a single Dirac cone on the surface," Nat. Phys. **5**(6), 438–442 (2009).
14. P. Yan, R. Lin, S. Ruan, A. Liu, H. Chen, Y. Zheng, S. Chen, C. Guo, and J. Hu, "A practical topological insulator saturable absorber for mode-locked fiber laser," Sci. Rep. **5**, 8690 (2015).
15. X. Mateos, P. Loiko, S. Y. Choi, F. Rotermund, M. Aguiló, F. Díaz, U. Griebner, and V. Petrov, "Single-walled carbon nanotubes oust graphene and semiconductor saturable absorbers in Q-switched solid-state lasers at 2 μm," Laser Phys. Lett. **14**(9), 095801 (2017).
16. M. Gaponenko, N. Kuleshov, and T. Südmeyer, "Passively Q-switched thulium microchip laser," IEEE Photonics Technol. Lett. **28**(2), 147–150 (2016).
17. R. Lan, X. Mateos, Y. Wang, J. M. Serres, P. Loiko, J. Li, Y. Pan, U. Griebner, and V. Petrov, "Semiconductor saturable absorber Q-switching of a holmium micro-laser," Opt. Express **25**(5), 4579–4584 (2017).
18. K. Scholle, S. Lamrini, P. Koopmann, and P. Fuhrberg, "2 μm laser sources and their possible applications," in *Frontiers in Guided Wave Optics and Optoelectronics*, B. Pal, ed. (Intech, 2010), pp. 471–500.
19. Z. Luo, C. Liu, Y. Huang, D. Wu, J. Wu, H. Xu, Z. Cai, Z. Lin, L. Sun, and J. Weng, "Topological-insulator passively Q-switched double-clad fiber laser at 2 μm wavelength," IEEE J. Sel. Top. Quantum Electron. **20**(5), 0902708 (2014).
20. J. Lee, M. Jung, J. Koo, C. Chi, and J. H. Lee, "Passively Q-switched 1.89-μm fiber laser using a bulk-structured Bi2Te3 topological insulator," IEEE J. Sel. Top. Quantum Electron. **21**(1), 0900206 (2015).
21. J. Bogusławski, G. Soboń, K. Tarnowski, R. Zybała, K. Mars, A. Mikuła, K. M. Abramski, and J. Sotor, "All-polarization-maintaining-fiber laser Q-switched by evanescent field interaction with Sb_2Te_3 saturable absorber," Opt. Eng. **55**(8), 081316 (2016).
22. J. M. Serres, P. Loiko, X. Mateos, K. Yumashev, U. Griebner, V. Petrov, M. Aguiló, and F. Díaz, "Tm:$KLu(WO_4)_2$ microchip laser Q-switched by a graphene-based saturable absorber," Opt. Express **23**(11), 14108–14113 (2015).
23. R. Lan, P. Loiko, X. Mateos, Y. Wang, J. Li, Y. Pan, S. Y. Choi, M. H. Kim, F. Rotermund, A. Yasukevich, K. Yumashev, U. Griebner, and V. Petrov, "Passive Q-switching of microchip lasers based on Ho:YAG ceramics," Appl. Opt. **55**(18), 4877–4887 (2016).
24. R. Zybala and K. T. Wojciechowski, "Anisotropy analysis of thermoelectric properties of $Bi_2Te_{2.9}Se_{0.1}$ prepared by SPS method," AIP Conf. Proc. **1449**(1), 393–396 (2012).
25. R. Zybała, K. Mars, A. Mikuła, J. Bogusławski, G. Soboń, J. Sotor, M. Schmidt, K. Kaszyca, M. Chmielewski, L. Ciupiński, and K. Pietrzak, "Synthesis and characterization of antimony telluride for thermoelectric and optoelectronic applications," Arch. Metall. Mater. **62**(2), 1067–1070 (2017).
26. J. Boguslawski, G. Sobon, R. Zybala, and J. Sotor, "Dissipative soliton generation in Er-doped fiber laser mode-locked by Sb_2Te_3 topological insulator," Opt. Lett. **40**(12), 2786–2789 (2015).
27. G. Hao, X. Qi, Y. Fan, L. Xue, X. Peng, X. Wei, and J. Zhong, "Spiral growth of topological insulator Sb_2Te_3 nanoplates," Appl. Phys. Lett. **102**(1), 013105 (2013).
28. K. A. Kokh, V. V. Atuchin, T. A. Gavrilova, N. V. Kuratieva, N. V. Pervukhina, and N. V. Surovtsev, "Microstructural and vibrational properties of PVT grown Sb_2Te_3 crystals," Solid State Commun. **177**, 16–19 (2014).
29. K. Takayama and M. Takashiri, "Multi-layered-stack thermoelectric generators using p-type Sb_2Te_3 and n-type Bi_2Te_3 thin films by radio-frequency magnetron sputtering," Vacuum **144**, 164–171 (2017).
30. J. Reimann, J. Güdde, K. Kuroda, E. V. Chulkov, and U. Höfer, "Spectroscopy and dynamics of unoccupied electronic states of the topological insulators Sb_2Te_3 and Sb_2Te_2S," Phys. Rev. B **90**(8), 081106 (2014).
31. K. Krzempek, D. Tomaszewska, and K. M. Abramski, "Dissipative soliton resonance mode-locked all-polarization-maintaining double clad Er:Yb fiber laser," Opt. Express **25**(21), 24853–24860 (2017).
32. K. Wang, H. Long, M. Fu, G. Yang, and P. Lu, "Intensity-dependent reversal of nonlinearity sign in a gold nanoparticle array," Opt. Lett. **35**(10), 1560–1562 (2010).
33. C. P. Wyss, W. Lüthy, H. P. Weber, V. I. Vlasov, Y. D. Zavartsev, P. A. Studenikin, A. I. Zagumennyi, and I. A. Shcherbakov, "Emission properties of a Tm^{3+}:$GdVO_4$ microchip laser at 1.9 μm," Appl. Phys. B **67**(5), 545–548 (1998).
34. P. A. Loiko, K. V. Yumashev, V. N. Matrosov, and N. V. Kuleshov, "Dispersion and anisotropy of thermo-optic coefficients in tetragonal $GdVO_4$ and YVO_4 laser host crystals: erratum," Appl. Opt. **54**(15), 4820–4822 (2015).

Optical Materials EXPRESS

35. A. S. Yasukevich, P. Loiko, N. V. Gusakova, J. M. Serres, X. Mateos, K. V. Yumashev, N. V. Kuleshov, V. Petrov, U. Griebner, M. Aguiló, and F. Díaz, "Modelling of graphene Q-switched Tm lasers," Opt. Commun. **389**, 15–22 (2017).
36. S. Chen, C. Zhao, Y. Li, H. Huang, S. Lu, H. Zhang, and S. Wen, "Broadband optical and microwave nonlinear response in topological insulator," Opt. Mater. Express **4**(4), 587–596 (2014).

1. Introduction

In recent years, various novel two-dimensional (2D) materials have been developed and manifested to be promising ultrafast broadband saturable absorbers (SAs) for near-IR lasers. The most prominent example is graphene, a 2D Dirac material based on a single layer of carbon atoms and exhibiting a unique zero bandgap feature which determines its broadband absorption [1]. Graphene was proved to possess a broadband saturable absorption with ultrafast recovery time τ_{rec} and relatively low saturation intensity I_{sat} [2,3] and it was applied in passively Q-switched (PQS) and mode-locked (ML) oscillators emitting at 1-2 μm. Moreover, carbon nanostructures, namely, single-walled carbon nanotubes (SWCNTs, rolled sheets of graphene) [4] or graphene oxide [5], as well as different layered 2D materials have been studied [6]. The latter are transition metal dichalcogenides (e.g., MoS_2) [7], black phosphorus [8], and topological insulators (TIs, e.g., Bi_2Te_3 or Sb_2Te_3) [9,10]. Such materials are formed of groups of atomic layers (quintuple Te-Sb-Te-Sb-Te for Sb_2Te_3) bound to each other by weak van-der-Waals forces, while in the layers the atoms are strongly bonded by covalent forces. The search of novel 2D materials as SAs is motivated by certain limitations inherent to graphene, namely, low fraction of the saturable losses (1.3% for a single carbon layer, from 2.3% of small-signal absorption) [11].

A topological insulator is a material which behaves like an insulator inside the material (bulk) but it has conducting states at the surface [12]. The band structure of these surface states is similar to that of graphene, showing a Dirac-like linear band dispersion [13], so that one can expect a broadband linear absorption feature from TIs. The surface states in TIs are symmetry protected, e.g., from the surface defects, by the time-reversal symmetry. When a TI is excited by high-intensity light with a photon energy ($h\nu$) higher than the TI bandgap, absorption saturation (bleaching) will be observed due to the Pauli blocking principle (finite number of electronic and hole states). This effect is similar to that in graphene so that one can expect a similar dependence of the saturation intensity on $h\nu$ (i.e., a decrease of I_{sat} for longer wavelengths [11]). Various materials have been studied as 2D TIs, such as Bi_2Te_3, Bi_2Se_3 and Sb_2Te_3. Saturable absorption of such TIs has been observed [9,14].

It is believed that 2D materials can become efficient "fast" SAs for ~2 μm PQS lasers. They are expected to enable the generation of ns-long pulses at intermediate repetition rates (hundreds of kHz – few MHz) [15]. Here, the classification is according to the relation between the characteristic time for the formation of a single Q-switched pulse ($\Delta\tau$) and τ_{rec}, so that the SAs can be classified as "slow" ($\Delta\tau << \tau_{rec}$) and "fast" ($\Delta\tau >> \tau_{rec}$) [15]. In this spectral range, there is a lack of reliable broadband "fast" SAs. Semiconductor SAs are commercially available and have been implemented in PQS ~2 μm lasers [15–17], however, they are expensive, show a limited spectral operation range (few tens of nm), and a moderate laser induced damage threshold (LIDT).

The relevance of the ~2 μm spectral range is because such an emission is eye-safe and it is used in remote sensing (LIDAR), wind mapping, spectroscopy, medicine and material (plastic) processing [18]. ~2 μm lasers are typically based on thulium (Tm^{3+}) and holmium (Ho^{3+}) ions. In the former case, the laser emission is due to the $^3F_4 \rightarrow {}^3H_6$ Tm^{3+} transition.

To date, most of the studies of ~2 μm lasers PQS with TIs as SAs have focused on fiber oscillators [19,20]. Recently, Wang *et al.* applied Sb_2Te_3 nanosheets prepared by facile hydrothermal reaction in a bulk $Yb:GdAl_3(BO_3)_4$ laser generating 0.92 μJ / 0.68 μs pulses at 1045 nm [10]. In the present work, we report on a successful application of a Sb_2Te_3 thin film as a SA in a microchip Tm laser emitting at ~1.9 μm. A similar SA was used previously in a

Optical Materials EXPRESS

PQS Er fiber laser [21]. The focus on the microchip laser is because this laser geometry is beneficial for obtaining nanosecond pulses when using 2D SAs [22,23].

2. Saturable absorber

2.1 Material preparation

Antimony telluride was synthesized using tellurium powder and antimony granules with purity >99.99%. A solid Sb_2Te_3 was obtained by alloying stoichiometric proportions of elementary powders in quartz ampoules sealed under vacuum (at 950 K for 1 h followed by slow cooling down). The furnace containing the ampoules was rocked during the process to ensure thorough mixing of the alloy components. Once cooled down, the obtained ingots were mechanically milled to obtain a powder and then sintered, using the Spark Plasma Sintering (SPS) technique [24], to produce a cathode for the subsequent deposition process. Thin films of Sb_2Te_3 were deposited using the pulsed magnetron sputtering technique (physical vapor deposition, PVD), see [25,26]. The deposition itself was performed using a single planar magnetron (WMK-50) driven by a DORA Power System in a standard batch-type vacuum system. The sputtering process was performed in a 0.25 Pa Ar atmosphere at current of 0.05 A and an effective power of 0.03 kW. Standard 1-inch glass substrates were employed, mounted on a rotatory table at 30 rpm inside a vacuum chamber.

2.2 Structural study

The as-synthesized thin films of Sb_2Te_3 were characterized using scanning electron microscopy (SEM), Raman spectroscopy, X-ray diffraction analysis (XRD) and profilometry. SEM images (Hitachi SU8230) are presented in Fig. 1(a,b) showing the surface of the deposited 15-nm-thick film. The obtained samples were smooth and characterized by good uniformity over a large area. The thickness of the films was determined using a Veeco Dektak 150 surface profiler, see Fig. 1(c). Samples with a film thickness from 3 to 15 nm were obtained.

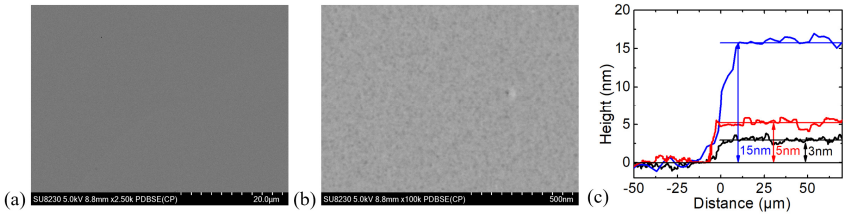

Fig. 1. (a,b) SEM images of the surface of a 15-nm-thick Sb_2Te_3 film on a glass substrate (scale bar: (a) 20 μm, (b) 500 nm); (c) the profilometer results showing 3 nm-, 5 nm- and 15 nm-thick films.

For Raman and XRD studies a thicker (2 μm) film was prepared on a SiO_2 substrate. The Raman spectra were collected using a Horiba LabRam HR800 spectrometer coupled with a 532 nm Nd:YAG laser. Measurements were carried out at several random points at the layer surface with following parameters: acquisition time of 10 s and 6 accumulations. The Raman spectra presented in Fig. 2(a) consist of 6 bands related to Sb_2Te_3 vibrations: 65, 87, ~117 cm^{-1} (containing two bands centered at 110 and 121 cm^{-1}), 137 and 162 cm^{-1}. The bands at 65, 110 and 162 cm^{-1} correspond to the A_{1g} and E_g normal modes of the Sb-Te vibrations [27], while the bands at 87, 121 and 137 cm^{-1} are related to Te-Te interactions between two quintuples which result from the packet structure of Sb_2Te_3 [28]. The small changes in relative intensities of the mentioned bands are related to a not perfectly smooth surface of the sample, however, all characteristic bands are clearly visible at all measurement points, which confirms a uniform morphology of the material.

Optical Materials EXPRESS

The XRD studies were performed using the Grazing Incidence Diffraction (GID) technique and a PANalytical Empyrean diffractometer with a parallel beam (at 1°) and an Euler's holder. The measured XRD pattern of a 2-μm-thick Sb_2Te_3 film deposited on a SiO_2 substrate is shown in Fig. 2(b). XRD confirms the presence of trigonal (space group D^5_{3d} - $R\bar{3}m$, No. 166) Sb_2Te_3 phase [29]. The lattice constants determined according to the 2θ position of the diffraction peaks are a = 4.76 Å, c = 29.26 Å. These values are slightly different from those for stoichiometric Sb_2Te_3 (a = 4.26 Å, c = 30.45 Å, PDF card No. 15-0874) which may indicate a certain sample non-stoichiometry. Applying the Scherrer formula to analyse the broadening of the diffraction peaks, we estimated the mean crystallite size as 18.4 nm.

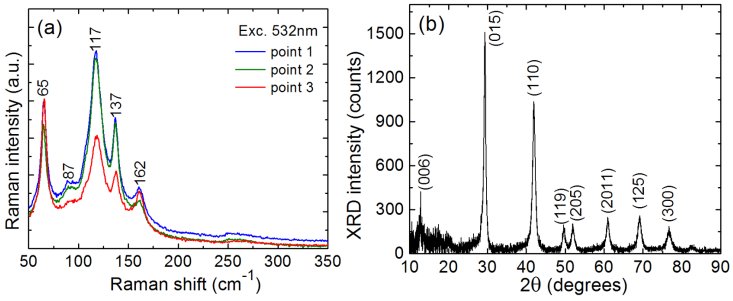

Fig. 2. Raman spectra at several random points (a) and XRD pattern (b) of a 2-μm-thick Sb_2Te_3 film deposited on a SiO_2 substrate.

Thus, our structural studies indicate that the prepared material has the form of mixed polycrystalline-amorphous thin films containing slightly non-stoichiometric nm-sized Sb_2Te_3 crystallites. Such a structure promotes the large density of the surface states which is desirable for TIs.

2.3 Linear and non-linear absorption

The small-signal transmission spectra of the prepared Sb_2Te_3 films are shown in Fig. 3(a) (the Fresnel losses due to the uncoated glass substrate were subtracted). The Sb_2Te_3 films are characterized by a broadband absorption in the near-IR (0.8-2.2 μm). The absorption increases with the thickness of the film. For the 3 nm-, 5 nm- and 15 nm-thick films, the small-signal transmission T_{SA} at ~1.9 μm is 99.5%, 99.0% and 96.3%, respectively. The photograph of the substrate with the 15 nm-thick Sb_2Te_3 film is shown in the inset of Fig. 3(a). The film has a uniform grey color.

The study of ultrafast electron dynamics for Sb_2Te_3 TI revealed a characteristic decay time of ~1 ps [30]. For PQS lasers for which the the characteristic time for the formation of a single Q-switched pulse is about several ns, Sb_2Te_3 is a "fast" SA.

The absorption saturation of Sb_2Te_3 thin film was studied using an open-aperture Z-scan method. The sample was translated along the focused beam of a pulsed (ns) laser (i.e., in the axial direction, along the z-axis) providing a variation of the incident peak intensity, see Ref [7] for the details. We used a stable dissipative soliton resonance ML Er,Yb fiber laser operating at 1560 nm and generating $\Delta\tau$ = 25 ns-long pulses with a near-square temporal profile at a pulse repetition frequency (PRF) of 1 MHz with a linear polarization [31]. The average output power P_{out} was 136 mW. The spot diameter at the focus $2w_L$ was ~10 μm allowing one to reach a maximum peak intensity $I = 2E/(\pi w_L^2 \Delta\tau)$ of >10 MW/cm^2 ($E = P_{out}$/PRF is the pulse energy).

Optical Materials EXPRESS

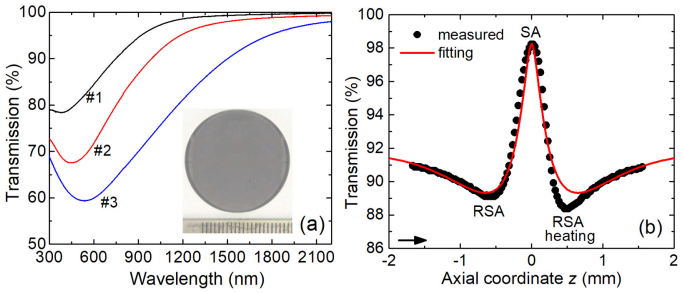

Fig. 3. (a) Small-signal transmission spectra of the 3 nm (#1), 5 nm (#2) and 15 nm (#3) thick Sb_2Te_3 SAs (Fresnel losses are subtracted), *inset* – photograph of the SA #3; (b) Open-aperture Z-scan curve for the SA #3 at 1560 nm, SA: saturable absorption; RSA: reverse saturable absorption. *Circles* – experimental data, *red curve* – their modelling with Eq. (1). *Arrow* indicates the direction of sample moving.

The open-aperture Z-scan curve for a 15 nm-thick Sb_2Te_3 film on a glass substrate is shown in Fig. 3(b). In the initial part, the transmission decreased by ~2% with increasing I. Reverse saturable absorption (RSA) feature can be associated, e.g., with two-photon absorption (TPA) [32]. The point of inflection corresponds to $I = 0.06$ MW/cm^2, after which the transmission increases by 9.2%. This type of the Z-scan curve was maintained when repeating the measurements in various sample points. The asymmetric shape of the curve is due to sample heating after passing the beam waist. To fit the measured Z-scan curve, we used the "fast" SA model [7] modified for the case of saturable TPA [32]. The small-signal sample transmission $T_{SA} = 1 - \alpha'_0$, where α'_0 is the small-signal absorption. The intensity dependence of $T(I)$ can be expressed as $1 - \alpha'(I)$, where:

$$\alpha'(I) = \alpha'_{NS} + \frac{\alpha'_S}{1+(I/I_{sat})} - \beta'(I), \text{where} \beta'(I) = \frac{\beta_0'}{1+(I/I_{TPA})}. \quad (1)$$

Here, $\alpha'(I)$ is the intensity-dependent total absorption, α'_{NS} is the non-saturable absorption, α'_S and I_{sat} are the saturable absorption and the saturation intensity, respectively, $\beta'(I)$ is the intensity-dependent TPA, β_0' is the small-signal TPA and I_{TPA} is the corresponding saturation intensity. Thus, for $I \to 0$, $\alpha'(0) = \alpha'_{NS} + \alpha'_S - \beta_0'$ and in the case of complete SA bleaching (for $I >> I_{sat}, I_{TPA}$), $\alpha'(\infty) = \alpha'_{NS}$. The Eq. (1) was used and the spatial and temporal distribution of the laser intensity was considered [7]. The results are shown in Fig. 3(b). The best-fit parameters are $I_{sat} = 0.17$ MW/cm^2, $\alpha'_S = 13.1\%$, $\alpha'_{NS} = 0.7\%$, $I_{TPA} = 8$ kW/cm^2, $\beta_0' = 5.6\%$. Thus, the fraction of the useful losses or "modulation depth" to the maximum total losses is rather high for the Sb_2Te_3 SA, namely $(\alpha'_S - \beta_0')/(\alpha'_{NS} + \alpha'_S) = 0.54$.

3. Laser experiments

3.1 Laser set-up

As a laser crystal, we used tetragonal gadolinium vanadate ($GdVO_4$) doped with Tm^{3+} (2 at.%). Tm:$GdVO_4$ is known as a suitable material for efficient ~2 μm diode-pumped lasers due to its attractive spectroscopic and thermal properties [33]. The laser crystal was cut for light propagation along the ***a***-axis (***a***-cut). It was 2.1-mm-thick with an aperture of 4.0 × 3.0 mm^2. Both its input and output faces were polished to laser quality and remained uncoated. The crystal was wrapped in In-foil to improve the thermal contact from all 4 lateral sides and mounted in a Cu-holder water-cooled to 12 °C.

Optical Materials EXPRESS

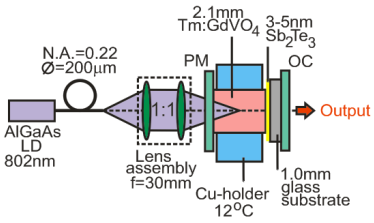

Fig. 4. Scheme of the Tm:$GdVO_4$/Sb_2Te_3 PQS microchip lasers: LD – laser diode, PM – pump mirror, OC – output coupler.

A microchip-type plano-plano laser cavity was used, Fig. 4. It is known that the $GdVO_4$ crystal has positive thermo-optic coefficients dn/dT [34] which determine a positive sign of the thermal lens. The latter provides mode stabilization (thermal guiding) in a plano-plano cavity. The plane pump mirror (PM) was coated for high transmission (HT) at 0.78–1.0 μm and for high reflection (HR) at 1.8–2.1 μm. A set of plane output couplers (OCs) with transmission T_{OC} ranging from 1% to 30% at 1.8–2.1 μm were used. For continuous-wave (CW) operation, both PM and OC were placed as close as possible to the laser crystal. For PQS operation, transmission-type SAs based on 3 nm and 5 nm-thick Sb_2Te_3 films on an uncoated glass substrate were inserted between the laser crystal and OC with minimum air gaps. The crystal was pumped using a fiber-coupled (numerical aperture, N.A. = 0.22, fiber core diameter: 200 μm) AlGaAs laser diode emitting unpolarized output at 802 nm. The diode output was collimated and focused into the crystal through the PM using a lens assembly (1:1 reimaging ratio, 30 mm focal length). The radius of the pump beam w_p was 100 μm. The pump absorption under lasing conditions was ~65%.

3.2 Continuous-wave laser

At first, we studied CW microchip laser operation of Tm:$GdVO_4$ with all OCs. The laser output was linearly polarized (σ-polarization). The polarization was naturally selected by the gain anisotropy. The input-output dependences are shown in Fig. 5(a).

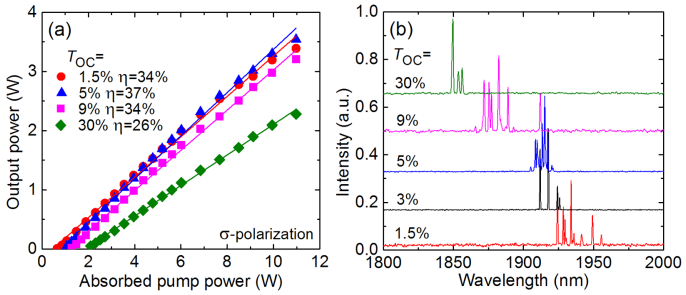

Fig. 5. CW Tm:$GdVO_4$ microchip laser: (a) input-output dependences, η – slope efficiency; (b) typical laser emission spectra for P_{abs} = 11.0 W.

The best performance corresponded to T_{OC} = 5%. The laser generated a maximum output power of 3.54 W at 1905-1921 nm with a slope efficiency η of 37% (with respect to the absorbed pump power P_{abs}). The laser threshold was at P_{abs} = 0.95 W. For higher output coupling the blue shift of the laser wavelength, in agreement with the quasi-three-level nature of the Tm^{3+} ions, was observed. The 2 μm emission band of Tm^{3+} ions overlaps with the absorption one (the $^3F_4 \leftrightarrow {}^3H_6$ transitions). The reabsorption losses (and, thus, the gain spectra) depend on the inversion ratio β which is determined by output coupling. Fog high T_{OC}, higher gain (higher β) is required to compensate the output-coupling losses. Thus, the gain spectra experience a blue-shift due to the decreased reabsorption. For the lowest T_{OC} = 1.5%, the laser operated at 1924-1956 nm, whether for the highest T_{OC} = 30% it operated at

Optical Materials EXPRESS

1849-1856 nm, Fig. 5(b). The laser emission showed a multi-peak behavior due to etalon (Fabry-Perot) effects.

3.3 Passively Q-switched laser

For the PQS laser, the output coupler with T_{OC} = 5% was selected as it provided better stability of the Q-switched operation. The laser output was σ-polarized. The results of the input-output dependences and the laser emission spectra of the PQS laser are shown in Fig. 6. For the 3 nm-thick Sb_2Te_3 SA, the maximum average output power reached 0.70 W at 1913 nm with η = 36%. The laser threshold was at P_{abs} = 1.05 W. The PQS conversion efficiency with respect to the output power in the CW operation mode η_{conv} was ~90%.

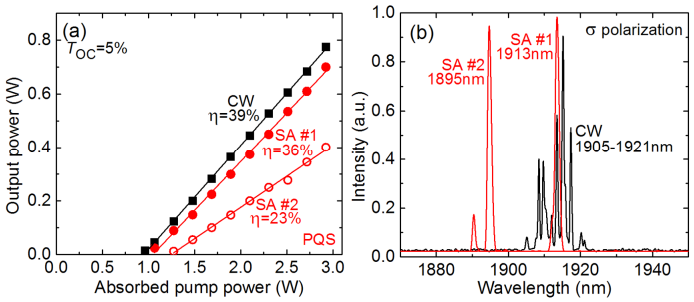

Fig. 6. Tm:$GdVO_4$ microchip laser PQS by Sb_2Te_3 SAs with a thickness of 3 nm (#1) and 5 nm (#2): (a) input-output dependences, η – slope efficiency; (b) typical laser emission spectra for P_{abs} = 2.9 W. The CW laser results in (a) are shown for comparison only in the narrow range of stable PQS operation where the slope efficiency is slightly higher compared to Fig. 5(a).

Physically, such a high value is related to (i) a high small-signal transmission of the SA at the laser wavelength, T_{SA} = 99.5%, (ii) high uniformity of the deposited Sb_2Te_3 film and (iii) small non-saturable loss of the Sb_2Te_3 SA, see Fig. 3(b). A small increase of the laser threshold and a relatively high η_{conv} indicate a small insertion loss for the Sb_2Te_3 SA. For P_{abs} > 3 W, Q-switching instabilities (e.g., multi-pulse behavior) were observed most probably due to the heating of the SA by the residual (non-absorbed) pump [22]. For P_{abs} < 3 W, no damage of the SA was observed.

For the thicker (5 nm) SA, the laser output deteriorated due to the higher insertion loss. The maximum output amounted to 0.40 W at the shorter wavelength of 1895 nm with η of only 23%. The laser threshold increased to P_{abs} = 1.25 W and η_{conv} was only 52%.

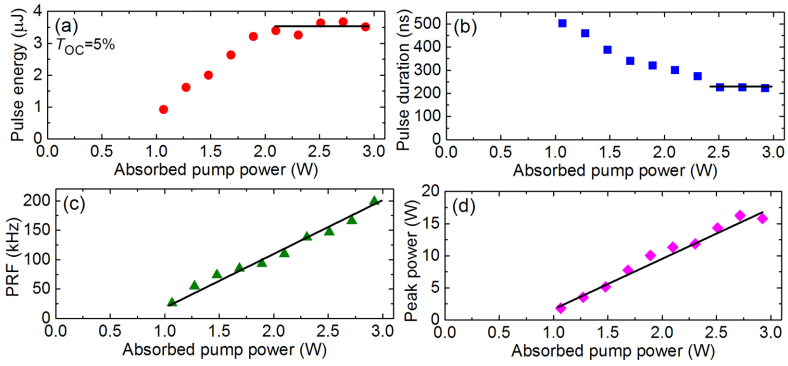

Fig. 7. Pulse energy (a), pulse duration (FWHM) (b), pulse repetition frequency (PRF) (c) and peak power (d) for the Tm:$GdVO_4$ microchip laser PQS with a 3 nm-thick Sb_2Te_3 SA.

The pulse characteristics of the PQS laser show a clear dependence on P_{abs}: the pulse duration $\Delta\tau$ (determined as FWHM) decreased from 502 to 223 ns, while the pulse energy E_{out} increased from 0.9 to 3.5 μJ, as shown in Fig. 7(a,b) for the 3 nm-thick SA. For absorbed

Optical Materials EXPRESS

pump powers well above the laser threshold (P_{abs} > 2 W), the dependence of the pulse characteristics on P_{abs} saturated. The pulse repetition frequency (PRF) varied almost linearly from 26 to 199 kHz, Fig. 7(c). The maximum peak power, $P_{peak} = E_{out}/\Delta\tau$, thus reached ~16 W, Fig. 7(d). Such a behavior is typical for "fast" SAs and it is related to a dynamic bleaching of the SA with P_{abs} [35]. A similar dependence of the pulse characteristics on P_{abs} was observed for the 5 nm-thick SA. At the maximum P_{abs} = 2.92 W, the laser generated 2.5 μJ / 230 ns pulses at a PRF of 160 kHz, so that the peak power was ~11 W.

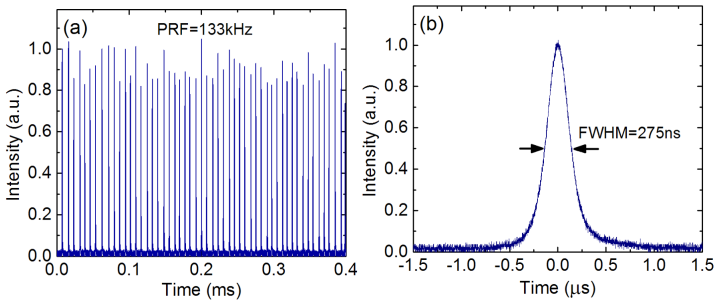

Fig. 8. Oscilloscope traces of the pulse train (a) and a single Q-switched pulse (b) from the Tm:$GdVO_4$ microchip laser PQS with a 3 nm-thick Sb_2Te_3 SA, P_{abs} = 2.3 W.

A typical pulse train from the PQS laser is shown in Fig. 8(a), exhibiting intensity instabilities <15%. They are related to the heating of the SA by the residual (non-absorbed) pump [22]. The latter can be eliminated by a dielectric coating (HR for the pump) of the crystal rear face. The corresponding oscilloscope trace of the single Q-switched pulse is presented in Fig. 8(b).

The high Q-switching conversion efficiency achieved in the present work (η_{conv} ~90% for 3 nm-thick Sb_2Te_3 film) is superior as compared to the previously studied "fast" SAs, i.e., graphene (35%), SWCNTs (53%), commercial semiconductor SAs (26%) [15] and few-layer MoS_2 [7] all employed in a similar Tm microchip laser based on a monoclinic Tm:$KLu(WO_4)_2$ crystal and emitting at ~1.94 μm.

In the present work, the Sb_2Te_3 thin-film SA was studied in the near-IR (at 1.56 μm for the absorption saturation and at 1.9 μm for the laser experiment). The corresponding photon energies are higher than the bulk bandgap of Sb_2Te_3 (0.21 eV). Thus, inter-band transitions across the bulk bandgap seem to have a significant contribution to the observed saturable absorption properties [36].

4. Conclusion

Thin films of Sb_2Te_3 are promising as "fast" saturable absorbers of passively Q-switched solid-state lasers emitting in the eye-safe spectral range near 2 μm. Deposition by pulsed magnetron sputtering provides low non-saturable losses and high uniformity of the film leading to a superior Q-switching conversion efficiency as compared, e.g., to such well-known "fast" SAs as graphene or SWCNTs. In the present work, we employed a Sb_2Te_3-based SA in a bulk microchip-type (thermally guided) laser based on a Tm:$GdVO_4$ crystal. We demonstrated the generation of nanosecond pulses at ~1.9 μm at high repetition rates (few hundreds of kHz). In particular, the PQS Tm:$GdVO_4$ microchip laser generated 3.5 μJ / 223 ns pulses at a repetition rate of ~200 kHz, corresponding to an average output power of 0.7 W and a slope efficiency of 36%. The Sb_2Te_3-based SAs are promising for passive Q-switching of waveguide (index-guided) lasers at ~2 μm based on evanescent field interaction, as the Sb_2Te_3 film can be directly deposited on various optical surfaces. For such lasers, <100 ns pulse durations and GHz-range repetition rates are expected.

Optical Materials EXPRESS

Funding

Spanish Government [MAT2016-75716-C2-1-R (AEI/FEDER, UE), TEC 2014-55948-R]; Generalitat de Catalunya (2014SGR1358); National Science Centre (NCN), Poland (UMO-2015/18/E/ST7/00296, UMO-2016/23/D/ST8/02686).

Acknowledgments

E. K. acknowledges financial support from the Generalitat de Catalunya under grants 2016FI_B00844 and 2017FI_B100158. F. D. acknowledges additional support through the ICREA academia award 2010ICREA-02 for excellence in research. J. B. acknowledges the doctoral fellowship financed by National Science Centre (NCN, Poland) under the grant no. 2016/20/T/ST7/00189. M. K. acknowledges the doctoral fellowship financed by National Science Centre (NCN, Poland) under the grant no. UMO-2017/24/T/ST7/00234. P. L. acknowledges financial support from the Government of the Russian Federation (Grant 074-U01) through ITMO Post-Doctoral Fellowship scheme. P.L. thanks Dr. Olga Dymshits for the help with the interpretation of the XRD pattern.

79.145.178.132 {ts '2020-05-12 08:32:51'}